Use of nonlinear journal-bearing impedance descriptions to evaluate linear analysis of the steady-state imbalance response for a rigid symmetric rotor supported by two identical finite-length hydrodynamic journal bearings at high eccentricities

Jean-Claude Luneno, Jan-Olov Aidanpää

Use of Nonlinear Journal Bearing Impedance Descriptions to Evaluate Linear Analysis of the Steady-State Unbalance Response for a Rigid Symmetric Rotor Supported by Two Identical Finite-length Hydrodynamic Journal Bearings at High Eccentricities

Jean-Claude Luneno
Luleå University of Technology, Sweden
E-mail: jean-claude.luneno@ltu.se
Tel: +46704573824
Fax: +46920491047

Jan-Olov Aidanpää
Luleå University of Technology, Sweden
E-mail: Jan-Olov.Aidanpaa@ltu.se

Abstract:

This paper concerns the investigation of linear models validity limits in predicting rotor trajectory inside the bearing clearance for a rigid symmetric rotor supported by two identical journal bearings operating at high eccentricities.
The inherent nonlinearity of hydrodynamic journal bearings becomes strong for eccentricities grater than 60 % of the bearing clearance where most existing linear models are not able to accurately predict the rotor trajectory.
The usefulness of nonlinear journal bearing impedance descriptions method in this investigation is due to the analytical formulations of the linearised bearing coefficients, and the analytical nonlinear bearing models. These analytically derived bearing coefficients do not require any numerical differentiation (or integration) and are therefore more accurate for large eccentricities. The analytically derived nonlinear bearing models markedly decrease the simulation time while valid for all L/D (length to diameter ratios) and all eccentricities.
The results contained in this paper show that linear models derived from the nonlinear impedance descriptions of the Moes cavitated (π − film) finite-length bearing can predict the steady-state unbalance response of a symmetric rigid rotor supported by two identical journal bearings at high eccentricities. This is, however, only the case when operating conditions are below the threshold speed of instability and when the system has period one solutions. The error will also become larger closer to the resonance speed.

Keywords: Nonlinear model, linear model, journal bearing, impedance descriptions, dynamics, unbalance response, rotor.

Nomenclature:

$C = C_r$	Bearing radial clearance [m]
$C_{ij}, i, j = X, Y$	Dimensional bearing damping coefficients [Ns/m]
$c_{ij}, i, j = X, Y$	Non-dimensional bearing damping coefficients [-]
D	Bearing inner diameter [m]
E	Rotor mass eccentricity [m]
e	Journal (rotor) dimensional eccentricity [m]
F_0	Half static load (for a symmetrically loaded rotor) [N]

F_x, F_y	Bearing reaction force $\hat{F}$ [N] components in the *x* and *y* directions
F_X, F_Y	Bearing reaction force $\hat{F}$ [N] components in the *X* and *Y* directions
g	Gravity acceleration [m/s^2]
$K_{ij}, i, j = X, Y$	Dimensional bearing stiffness coefficients [N/m]
$k_{ij}, i, j = X, Y$	Non-dimensional bearing stiffness coefficients [-]
$\hat{k}$	Unit vector in *z* and *Z* directions. [-]
L	Bearing length [m]
M	Rotor mass [kg]
O_1	Bearing centre
O_2	Rotor (journal) centre
R	Bearing inner radius [m]
rpm	Round per minute
S	Sommerfeld number [-]
t	Time [s]
$\hat{V}_j$	Journal (rotor) velocity vector [m/s]
$\hat{V}_S$	Journal's pure-squeeze-velocity vector [m/s]
V_S	Journal's pure-squeeze-velocity magnitude [m/s]
W_0	Bearing impedance $\hat{W}$ magnitude at the static equilibrium position
W_x, W_y	Bearing impedance $\hat{W}$ magnitude components in *x, y* directions
x,y,z	Coordinate system with abscise (*x-axis*) fixed to the vector $\hat{V}_S$, rotating with $\overline{\omega}$ relative to rotor inertial coordinates X, Y, Z
X,Y	Rotor displacement components in *X* and *Y* directions [m]
$\dot{X}, \dot{Y}$	Rotor velocity components in *X* and *Y* directions
$\ddot{X}, \ddot{Y}$	Rotor acceleration components in *X* and *Y* directions
$\overline{X}, \overline{Y}$	Rotor non-dimensional displacement components in *X* and *Y* directions [-]
$\overline{X}', \overline{Y}'$	Rotor non-dimensional velocity components in *X* and *Y* directions
$\overline{X}'', \overline{Y}''$	Rotor non-dimensional acceleration components in *X* and *Y* directions
γ	Journal (rotor) attitude angle [radians]
γ_0	Journal (rotor) attitude angle at static equilibrium position
ε	Journal (rotor) non-dimensional eccentricity [-]
$\hat{\varepsilon}$	Journal (rotor) non-dimensional eccentricity vector
ε_0	Journal (rotor) non-dimensional eccentricity at static equilibrium position
ς	Angle between *x* and *X* [radians]
μ	Oil dynamic viscosity [Pa×s]
ω	Rotor angular speed [rad/s]
$\overline{\omega}$	$\overline{\omega} = \frac{\omega}{2}$, is the angular speed of *x,y,z* coordinates relative to *X,Y,Z* [radians/s]

Introduction:

Undercritical industrial heavy rotating machinery sometimes operates at high eccentricities, for example hydropower or steam turbine with horizontal rotors. Therefore high eccentricity dynamic analysis of rotor-bearing systems is of industrial interest.
Linear models are widely used in most industrial design processes due to their simplicity and the ease with which it is possible to interpret the results. In the area of rotor-bearing system dynamics, most developed linear bearing models derived from the numerical differentiation approach are proved valid enough at low eccentricities.
In predicting the critical mass for a rigid symmetric rotor, Ram Turaga, A. S. Sekhar
and B. C. Majumdara [1] used the finite element method to calculate the bearing coefficients and found that linear models were valid for eccentricities less than 0.6.
A. K. Tieu and Z. L. Qiu [2] used Lund's infinitesimal perturbation method [3] and found that the rotor trajectory by the linear analysis assumes a significant error already at eccentricity 0.6 when the whirl amplitude is greater than 20 percent of the bearing clearance.
D. Childs [4] and Lund (1966) have demonstrated that the rotor is completely stable for eccentricities grater than 75 percent of the bearing clearance and for all L/D ratios.
Bearings with low L/D ratios in particular are more stable than others [6], therefore they will be the object of the present work, using L/D = 0.25.
R D Brown, G Drummond and P S Addison [5] showed that a rigid rotor supported on a hydrodynamic bearing film at high eccentricity satisfied the conditions for chaos.
Linear models are not valid for motions other than period one, therefore a bifurcation diagram is needed to locate such operating conditions and validate linear models outside these regions.
The purpose of this paper is to use the journal bearing impedance descriptions method for both linear and nonlinear models of bearing reaction forces to investigate how well linear models can approximate nonlinear models at high eccentricities.
The high nonlinear characteristics of bearing reaction forces at large eccentricities makes both numerical differentiation and integration approaches less accurate to linearise the bearing reaction forces [6].

Method

D. Childs, H. Moes, H. van Leeuwen [6], D. Childs [4] and H. Moes and R. Bosma [7] derived the journal impedance descriptions for rotordynamic applications, which consist of defining the bearing reaction force components as analytical nonlinear functions of the journal motion (displacement and velocity). They also derived the analytical bearing stiffness and damping coefficients by linearisation of the bearing reaction forces using Taylor series expansion; where second and higher order differential terms have been dropped. These analytical expressions for bearing coefficients are particularly suitable for rotordynamics work because they yield more accurate results and less computational time than the existing numerical differentiation and pressure-integration approaches. They also provide very accurate models for all eccentricities and L/D ratios.
The Moes cavitated ($\pi - film$) finite-length bearing model [7] will be used for present studies, with the following impedance (dimensionless bearing-load-force vector due to pure squeezing) components:

$$W_x \approx 6\left(1-\varepsilon^2\right)^{-1}\left(\left\{\left(1-y^2\right)T+x\right\}^{-1}+\left\{3^{-1}\left(1+2x^2-y^2\right)T+x\right\}^{-1}\left(1-\varepsilon^2\right)\left(\frac{L}{D}\right)^{-2}\right)^{-1}$$

$$W_y \approx 6y\left(1-\varepsilon^2\right)^{-1}\left(\left\{xT+1+\left(3\pi-4\right)2^2E\right\}^{-1}+\left\{xT+1-3^{-1}E\right\}^{-1}\left(1-\varepsilon^2\right)\left(\frac{L}{D}\right)^{-2}\right)^{-1}$$

$$T = 2\left(1-\varepsilon^2\right)^{\frac{1}{2}}\tan^{-1}\left(\left(1-\varepsilon^2\right)^{\frac{1}{2}}\left\{\left(1-y^2\right)^{\frac{1}{2}}-x\right\}^{-1}\right)$$

$$E = \left(1-\varepsilon^2\right)\left(1-y^2\right)^{-1}$$

$$\varepsilon = \frac{e}{C} = \sqrt{x^2+y^2} < 1$$

The dimensional bearing reaction forces in x and y directions are:

$$F_x = -V_s\,2\mu L\left(\frac{R}{C}\right)^3 W_x$$

$$F_y = -V_s\,2\mu L\left(\frac{R}{C}\right)^3 W_y$$

Transformation to the rotor fixed reference coordinates X, Y, Z is carried out as follows:

$$x = \frac{X\cos\varsigma + Y\sin\varsigma}{C}$$

$$y = \frac{Y\cos\varsigma - X\sin\varsigma}{C}$$

$$\varsigma = \tan^{-1}\left(\frac{\dot{Y}-\overline{\omega}X}{\dot{X}+\overline{\omega}Y}\right)$$

$$V_s = \left|\hat{V}_S\right| = \left|\hat{V}_j - \overline{\omega}\hat{k}\times C\hat{\varepsilon}\right| = \left\{\left(\dot{X}+\overline{\omega}Y\right)^2+\left(\dot{Y}-\overline{\omega}X\right)^2\right\}^{\frac{1}{2}}$$

$$\hat{V}_j = \begin{bmatrix}\dot{X} & \dot{Y} & 0\end{bmatrix}^T,\ \overline{\omega}\hat{k} = \begin{bmatrix}0 & 0 & \overline{\omega}\end{bmatrix}^T,\ C\hat{\varepsilon} = \begin{bmatrix}X & Y & 0\end{bmatrix}^T$$

$$\overline{\omega} = \frac{\omega}{2}$$

Vectors $\hat{V}_j, \hat{V}_S, C\hat{\varepsilon}, \hat{W}, \hat{F}$ and angles γ, ς are illustrated in Fig 17 in Appendix A.

The dimensional bearing reaction forces in X and Y directions are:

$$\begin{aligned} F_X &= F_x\cos(\varsigma) - F_y\sin(\varsigma) \\ F_Y &= F_x\sin(\varsigma) + F_y\cos(\varsigma) \end{aligned} \qquad \ldots (1)$$

The above bearing reaction forces are nonlinear functions of rotor displacement and velocity in the bearing clearance.

Modelling

A rigid symmetric rotor is supported by two identical plain cylindrical journal bearings with coordinates and parameters as shown in the figure below:

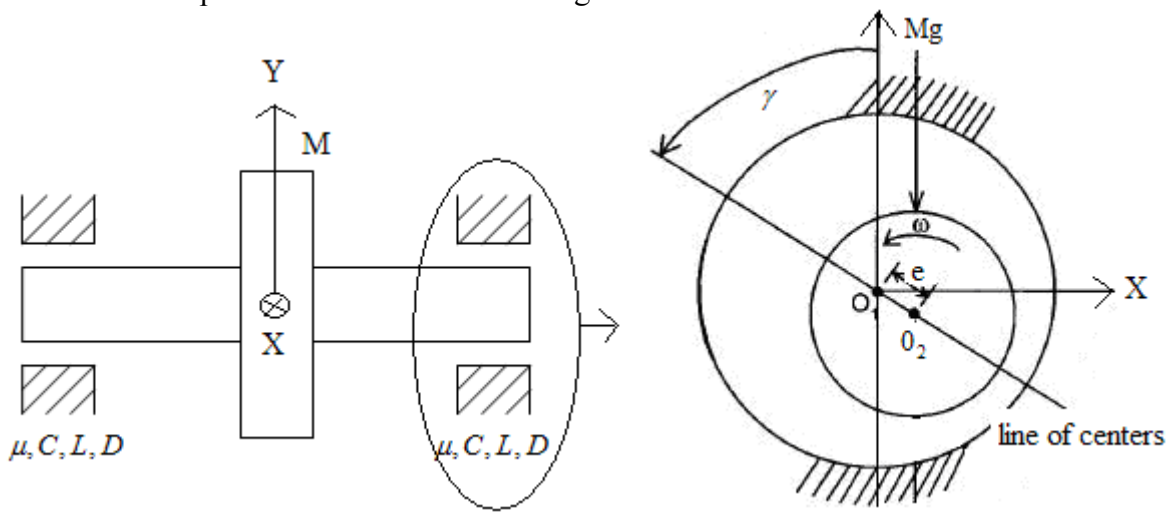

Fig 1. Rigid symmetric rotor supported by two identical plain cylindrical journal bearings

1) Nonlinear bearing model

Equations of motion

For an unbalanced rigid symmetric rotor supported by two identical journal bearings, the equations of motion of the rotor mass centre are:

$$\ddot{X} = \frac{2}{M} F_X + E\omega^2 \cos(\omega t)$$
$$\ddot{Y} = \frac{2}{M} F_Y + E\omega^2 \sin(\omega t) - g \qquad \text{... (2)}$$

where $M, F_X, F_Y, E, \omega, t, g$ are rotor mass (kg), bearing reaction force (N) in the X direction, bearing reaction force (N) in the Y direction, rotor mass eccentricity (m), rotor rotational speed (rad/s), time (s) and gravity acceleration (m/s^2) respectively.

2) Linear bearing model

The bearing reaction forces F_X, F_Y in equations (2) are linearised about the equilibrium position and are expressed as linear functions of rotor displacement and velocity.

Equations of motion about the equilibrium position

$$\begin{Bmatrix} \ddot{X} \\ \ddot{Y} \end{Bmatrix} = -\frac{2}{M}\left(\begin{bmatrix} C_{XX} & C_{XY} \\ C_{YX} & C_{YY} \end{bmatrix} \begin{Bmatrix} \dot{X} \\ \dot{Y} \end{Bmatrix} + \begin{bmatrix} K_{XX} & K_{XY} \\ K_{YX} & K_{YY} \end{bmatrix} \begin{Bmatrix} X \\ Y \end{Bmatrix} \right) + E\omega^2 \begin{Bmatrix} \cos\omega t \\ \sin\omega t \end{Bmatrix} \qquad \text{... (3)}$$

Introducing the dimensionless variables: $\begin{cases} \overline{X} = \dfrac{X}{C}, \overline{X}' = \dfrac{\dot{X}}{\omega C}, \overline{X}'' = \dfrac{\ddot{X}}{\omega^2 C} \\ \overline{Y} = \dfrac{Y}{C}, \overline{Y}' = \dfrac{\dot{Y}}{\omega C}, \overline{Y}'' = \dfrac{\ddot{Y}}{\omega^2 C} \\ \tau = \omega t \end{cases}$

Equations (3) can be written in non-dimensional form as follows:

$$p^2 \begin{Bmatrix} \overline{X}'' \\ \overline{Y}'' \end{Bmatrix} = -\left(\begin{bmatrix} c_{XX} & c_{XY} \\ c_{YX} & c_{YY} \end{bmatrix} \begin{Bmatrix} \overline{X}' \\ \overline{Y}' \end{Bmatrix} + \begin{bmatrix} k_{XX} & k_{XY} \\ k_{YX} & k_{YY} \end{bmatrix} \begin{Bmatrix} \overline{X} \\ \overline{Y} \end{Bmatrix} \right) + p^2 \left(\frac{E}{C} \right) \begin{Bmatrix} \cos\tau \\ \sin\tau \end{Bmatrix} \quad \ldots (4)$$

Where $p^2 = \dfrac{C\omega^2}{g}$, and the 8 non-dimensional bearing coefficients are obtained according to [6] as follows:

$$k_{XX} = \frac{\cos\gamma_0}{\varepsilon_0} - \sin\gamma_0 \left(\frac{\partial\gamma}{\partial\varepsilon} \right)_\alpha$$

$$k_{XY} = \frac{\sin\gamma_0}{\varepsilon_0} + \cos\gamma_0 \left(\frac{\partial\gamma}{\partial\varepsilon} \right)_\alpha$$

$$k_{YX} = \frac{-\sin\gamma_0}{\varepsilon_0} - \frac{\sin\gamma_0}{W_0} \left(\frac{\partial W}{\partial\varepsilon} \right)_\alpha$$

$$k_{YY} = \frac{\cos\gamma_0}{\varepsilon_0} + \frac{\cos\gamma_0}{W_0} \left(\frac{\partial W}{\partial\varepsilon} \right)_\alpha$$

$$c_{XX} = \frac{2\sin\gamma_0}{\varepsilon_0} \left(\frac{\partial\gamma}{\partial\alpha} \right)_\varepsilon$$

$$c_{XY} = \frac{-2\cos\gamma_0}{\varepsilon_0} \left(\frac{\partial\gamma}{\partial\alpha} \right)_\varepsilon$$

$$c_{YX} = \frac{2}{\varepsilon_0} \left[\cos\gamma_0 + \frac{\sin\gamma_0}{W_0} \left(\frac{\partial W}{\partial\alpha} \right)_\varepsilon \right]$$

$$c_{YY} = \frac{2}{\varepsilon_0} \left[\sin\gamma_0 - \frac{\cos\gamma_0}{W_0} \left(\frac{\partial W}{\partial\alpha} \right)_\varepsilon \right] \quad \ldots (5)$$

The partial derivatives required to evaluate the above coefficients (equations (5)) are found in Appendix B and the complete expressions for γ_0, W_0 are found in Appendix A.

At static equilibrium, the Sommerfeld number is:

$$S = \mu\left(\frac{\omega}{2\pi}\right)\left(\frac{R}{C}\right)^2 \frac{DL}{F_0} = \frac{1}{\pi\varepsilon_0 W_0} > 0\,, \quad \text{Or} \quad f(\varepsilon_0) = \mu\left(\frac{\omega}{2\pi}\right)\left(\frac{R}{C}\right)^2 \frac{DL}{F_0} - \frac{1}{\pi\varepsilon_0 W_0} = 0 \qquad \ldots (6)$$

Equation (6) is a nonlinear function of ε_0 to be solved in the interval $]0...1[$.

A case example

Some of the following data used for simulations are taken from [8] where a short-bearing solution was assumed. Results in [8] for eccentricities ($\varepsilon < 0.7$) were compared with results obtained using the nonlinear finite-length bearing impedance descriptions method.
For investigating high eccentricities ($\varepsilon > 0.7$) the bearing radial clearance C was doubled, and the short bearing solution was no longer valid:

$M = 22.6796$ [Kg], $R = 2.54\times10^{-2}$ [m], $D = 2\times R$, $L = 0.5\times R$, $\frac{L}{D} = 0.25$,

$C = 101.6\times10^{-6}$ [m], $\mu = 0.0069$ [$Pa\times s$], $E = 8.128\times10^{-6}$ [m]

Results

The results shown in Fig 2 and Fig 3 are the bifurcation diagrams for the system with a nonlinear bearing model. In these bifurcation diagrams (not maximum or minimum displacements) the rotational speed is increased in steps of 100 rpm and 100 Poincaré sections are plotted after the transients have decayed, 200 periods from start.

Figures 4 to 10 display the steady-state unbalance response solutions of equations (2) for the system with a nonlinear bearing model (blue), and the steady-state unbalance response solutions of equations (4) for the system with a linear bearing model (red). The solutions are presented as rotor trajectories plots for the selected rotational speeds of interest, 1000, 2000, 3000, 6000, 6300, 7700, 11000 rpm.

Figures 11 and 12 show the differences between the maximum absolute values of $\overline{X}$ and $\overline{Y}$ displacements of steady-state solutions of equations (2) and (4) for a range of rotational speeds from 5000 rpm to 10000 rpm.

Figures 13 and 14 are the bifurcation diagrams and steady-state unbalance response respectively. These results were obtained by using data from [8] where the bearing radial clearance $C = 50.8\times10^{-6}$ [m] is half of that used in the case example studied. The bifurcation diagrams in Fig 13 differ markedly from those in Fig 2 and Fig 3. The bearing radial clearance is the only parameter changed to obtain the resulting differences.

Equations (2) and (4) were numerically integrated using the 5th order Runge-Kutta numerical integration method with adaptive integration time steps.
Equations (3) were transformed into non-dimensional form (equations (4)) just for numerical convenience using the derived bearing coefficients in their non-dimensional form. The dimensional solutions (*X, Y* displacements) of equations (2) are converted to their non-dimensional quantities by dividing by the bearing clearance *C*.

The initial conditions for X and Y variables were to be chosen in the interval $]0\ldots C[$ for the numerical integration of equations (2) and for the numerical integration of equations (4) the initial conditions were $(\overline{\mathrm{X}}_0, \overline{\mathrm{Y}}_0)$. The remaining initial conditions for velocities $\dot{X}_0 = \dot{Y}_0 = \overline{X}_0' = \overline{Y}_0' = 0$.

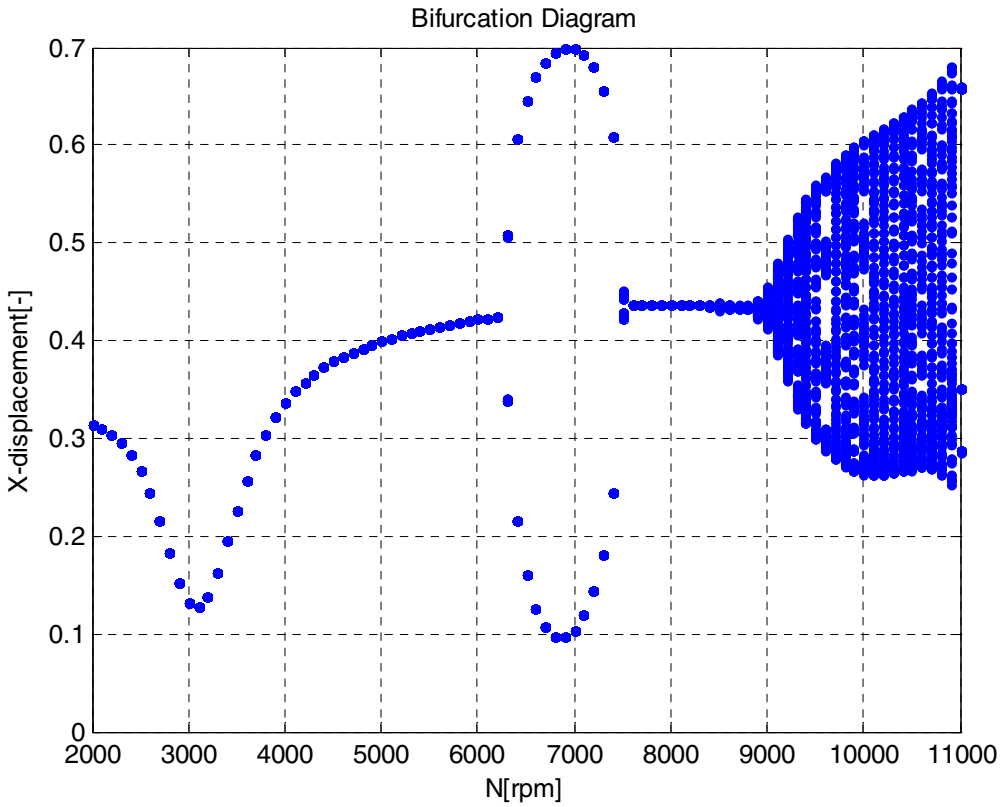

Fig 2. X displacements bifurcation diagram for the case example studied

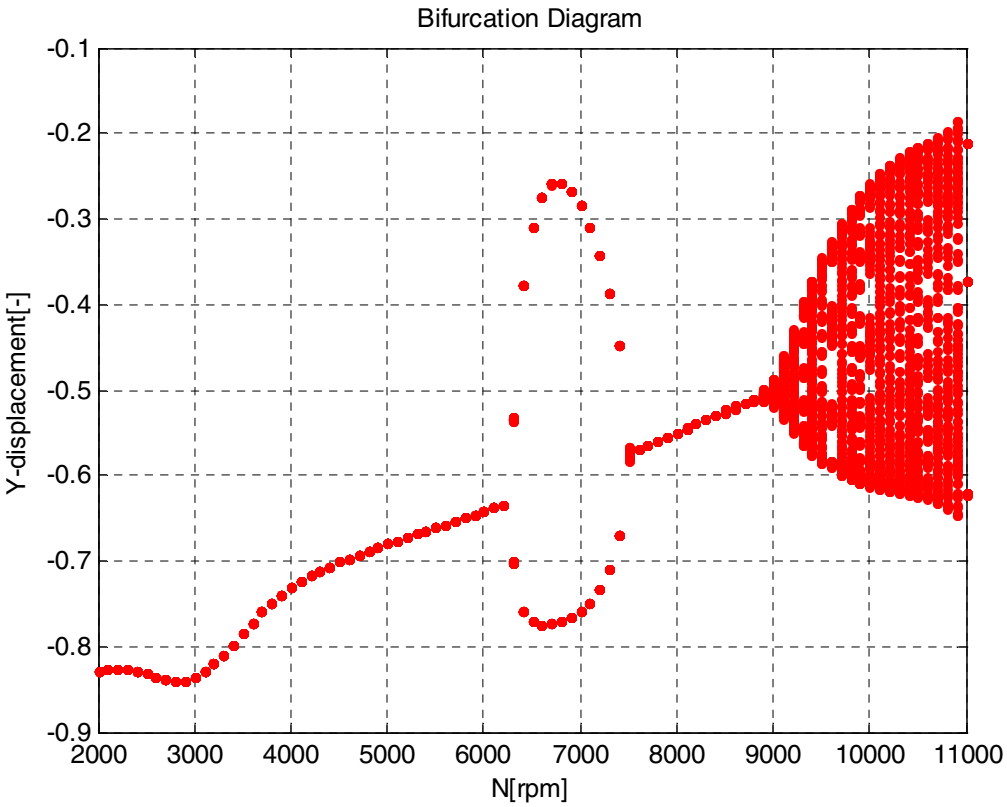

Fig 3. *Y* displacements bifurcation diagram for the case example studied

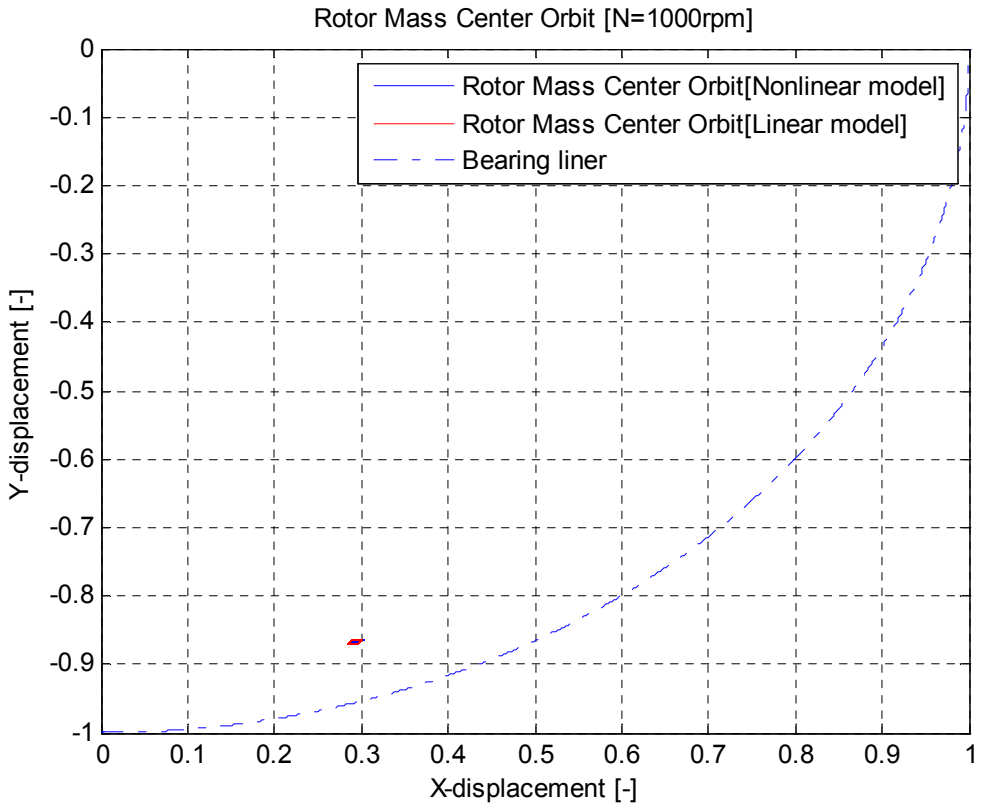

Fig 4a. Steady-state unbalance response solutions of equations (2) for the system with a nonlinear bearing model (blue) and the steady-state unbalance response solution of equations (4) for the system with a linear bearing model (red) at rotor speed of 1000 rpm. The rotor non-dimensional coordinates at static equilibrium position are:
$\overline{X}_0 = 0.2928, \overline{Y}_0 = -0.8669, \varepsilon_0 = 0.919241$

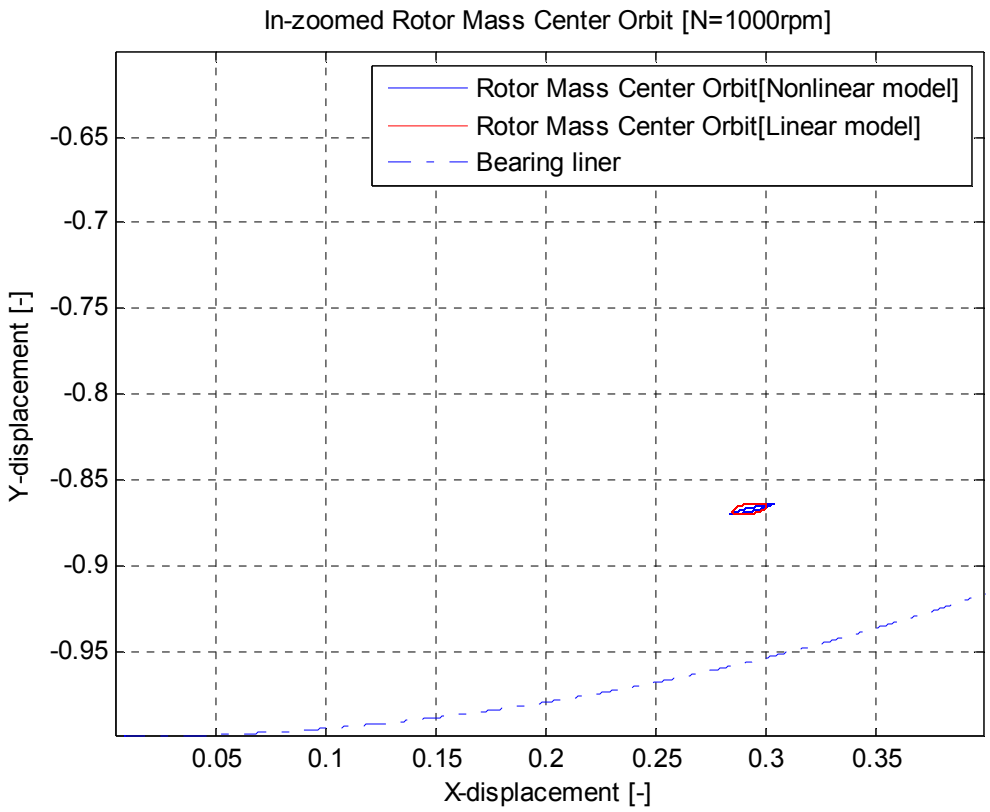

Fig 4b. In-zoomed Fig 4a

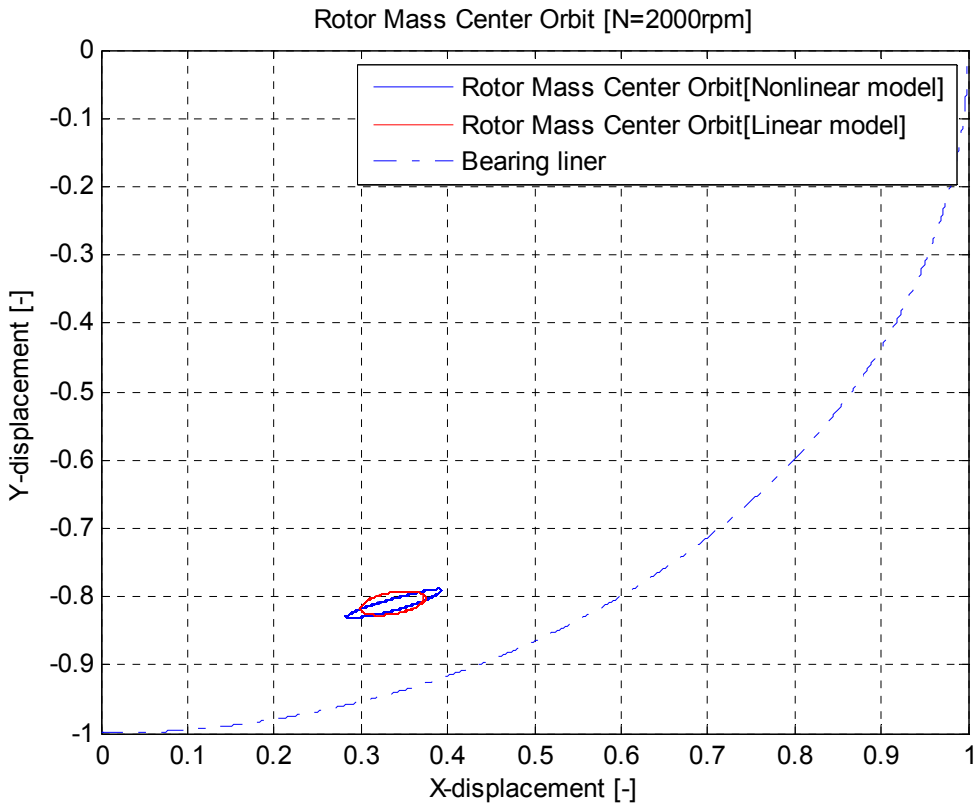

Fig 5. Steady-state unbalance response solutions of equations (2) for the system with a nonlinear bearing model (blue) and the steady-state unbalance response solution of equations (4) for the system with a linear bearing model (red) at rotor speed of 2000 rpm. The rotor non-dimensional coordinates at static equilibrium position are:
$\overline{X}_0 = 0.3366, \overline{Y}_0 = -0.8101, \varepsilon_0 = 0.882644$

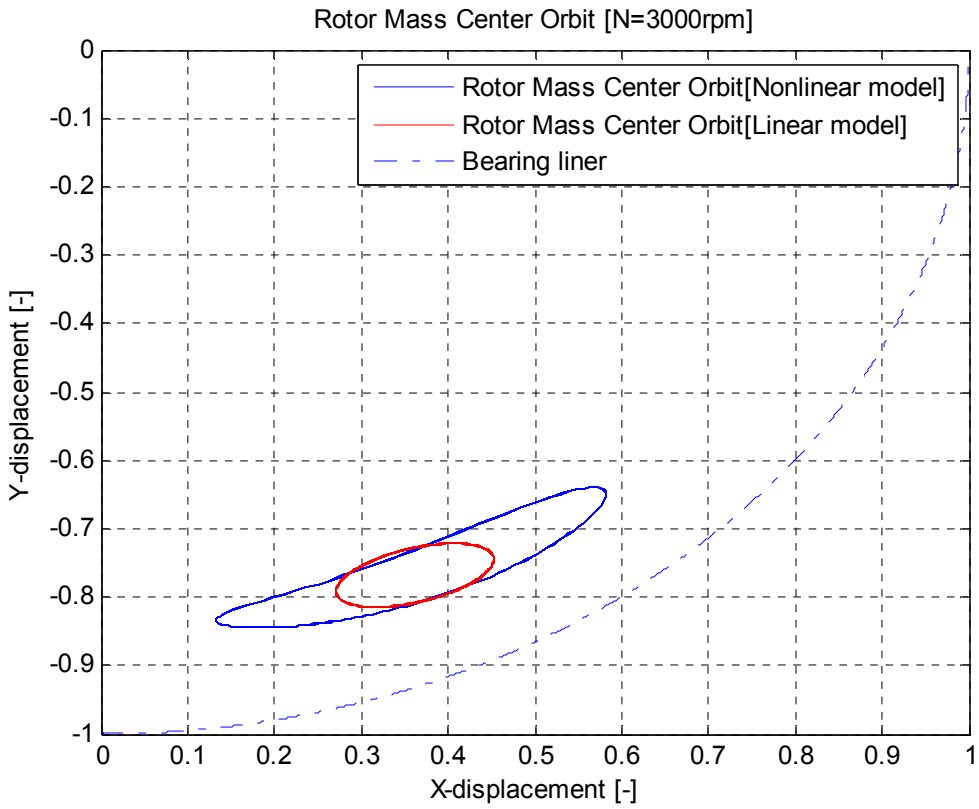

Fig 6. Steady-state unbalance response solutions of equations (2) for the system with a nonlinear bearing model (blue) and the steady-state unbalance response solution of equations (4) for the system with a linear bearing model (red) at rotor speed of 3000 rpm. The rotor non-dimensional coordinates at static equilibrium position are:
$\overline{X}_0 = 0.3616, \overline{Y}_0 = -0.7679, \varepsilon_0 = 0.855044$

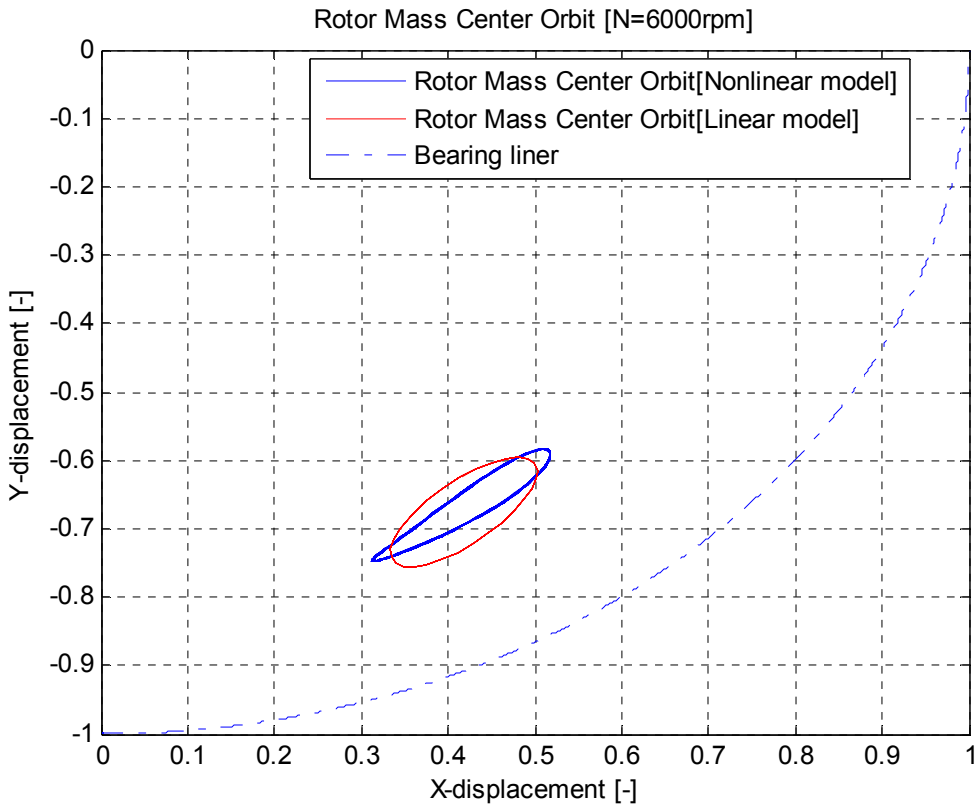

Fig 7. Steady-state unbalance response solutions of equations (2) for the system with a nonlinear bearing model (blue) and the steady-state unbalance response solution of equations (4) for the system with a linear bearing model (red) at rotor speed of 6000 rpm. The rotor non-dimensional coordinates at static equilibrium position are:
$\overline{X}_0 = 0.4182$, $\overline{Y}_0 = -0.6755$, $\varepsilon_0 = 0.7945$

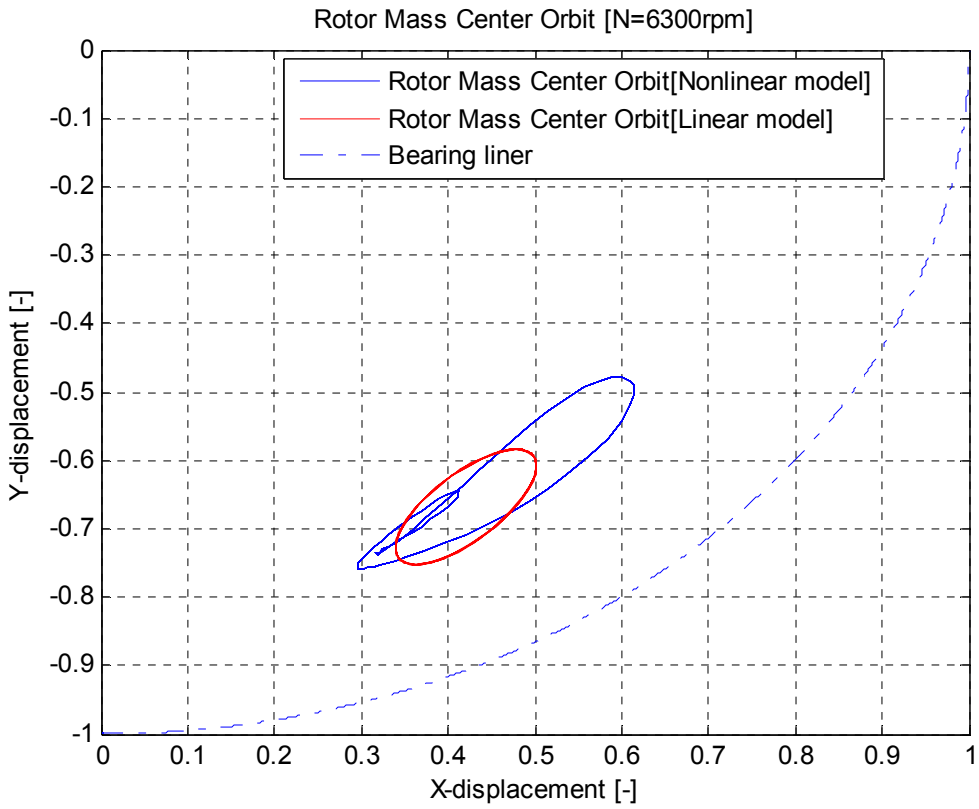

Fig 8. Steady-state unbalance response solutions of equations (2) for the system with a nonlinear bearing model (blue) and the steady-state unbalance response solution of equations (4) for the system with a linear bearing model (red) at rotor speed of 6300 rpm. The rotor non-dimensional coordinates at static equilibrium position are:
$\overline{X}_0 = 0.4205, \overline{Y}_0 = -0.6682, \varepsilon_0 = 0.7895$

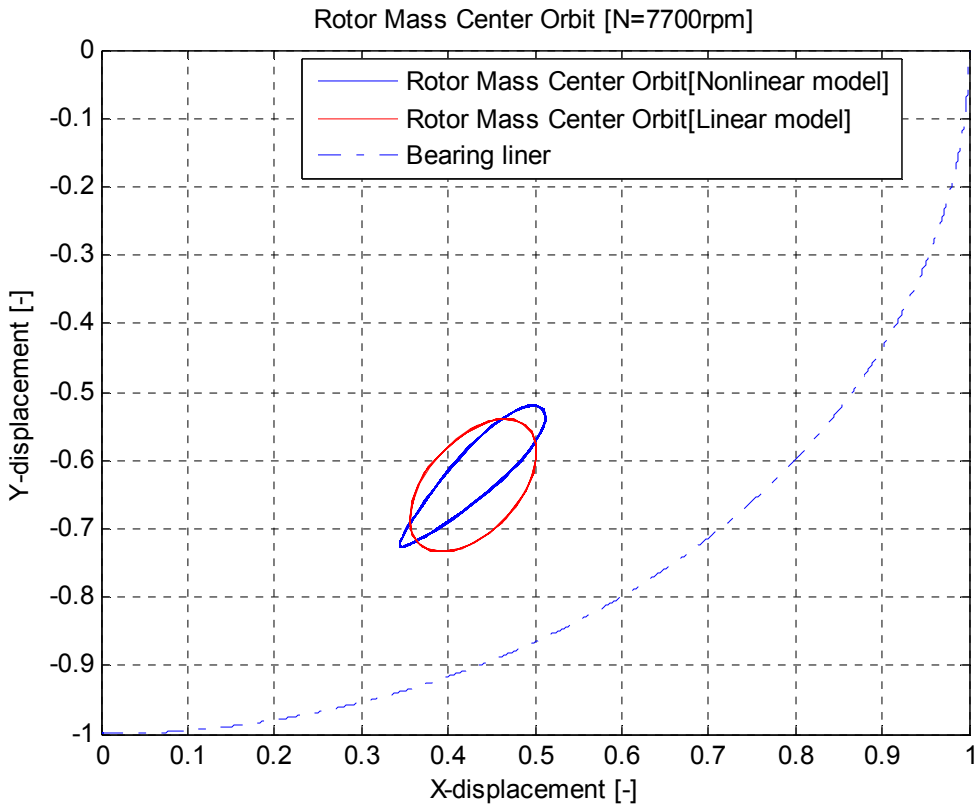

Fig 9. Steady-state unbalance response solutions of equations (2) for the system with a nonlinear bearing model (blue) and the steady-state unbalance response solution of equations (4) for the system with a linear bearing model (red) at rotor speed of 7700 rpm. The rotor non-dimensional coordinates at static equilibrium position are:
$\overline{X}_0 = 0.4290, \overline{Y}_0 = -0.6366, \varepsilon_0 = 0.7677$

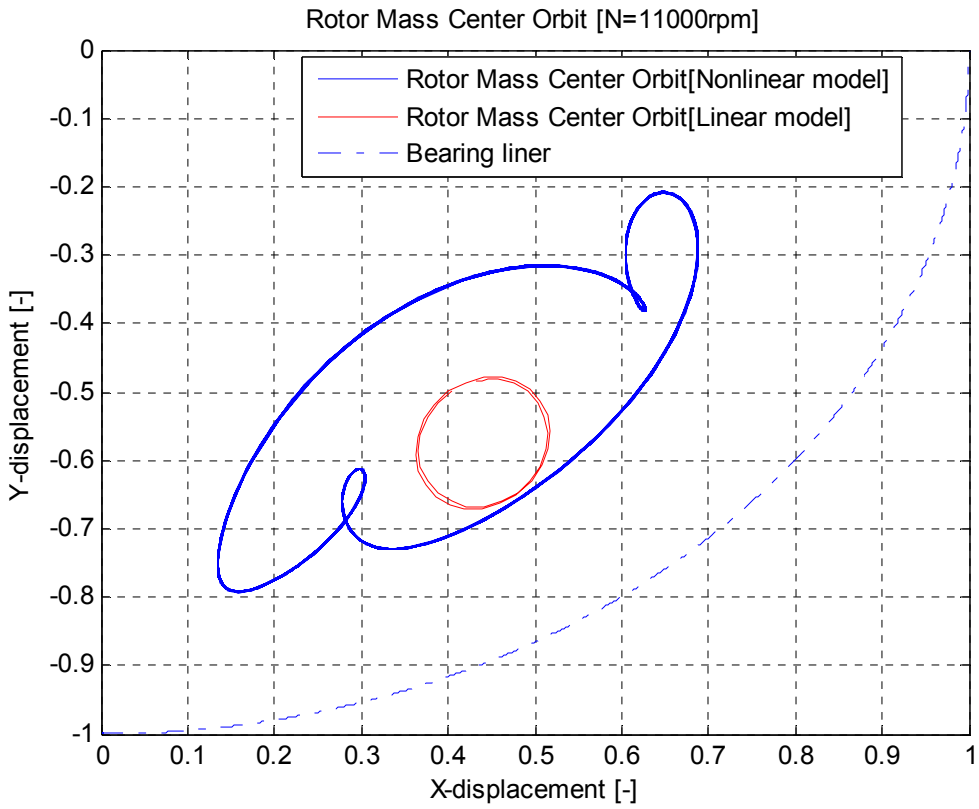

Fig 10. Steady-state unbalance response solutions of equations (2) for the system with a nonlinear bearing model (blue) and the steady-state unbalance response solution of equations (4) for the system with a linear bearing model (red) at rotor speed of 11000 rpm. The rotor non-dimensional coordinates at static equilibrium position are:
$\overline{X}_0 = 0.4404, \overline{Y}_0 = -0.5750, \varepsilon_0 = 0.7243$

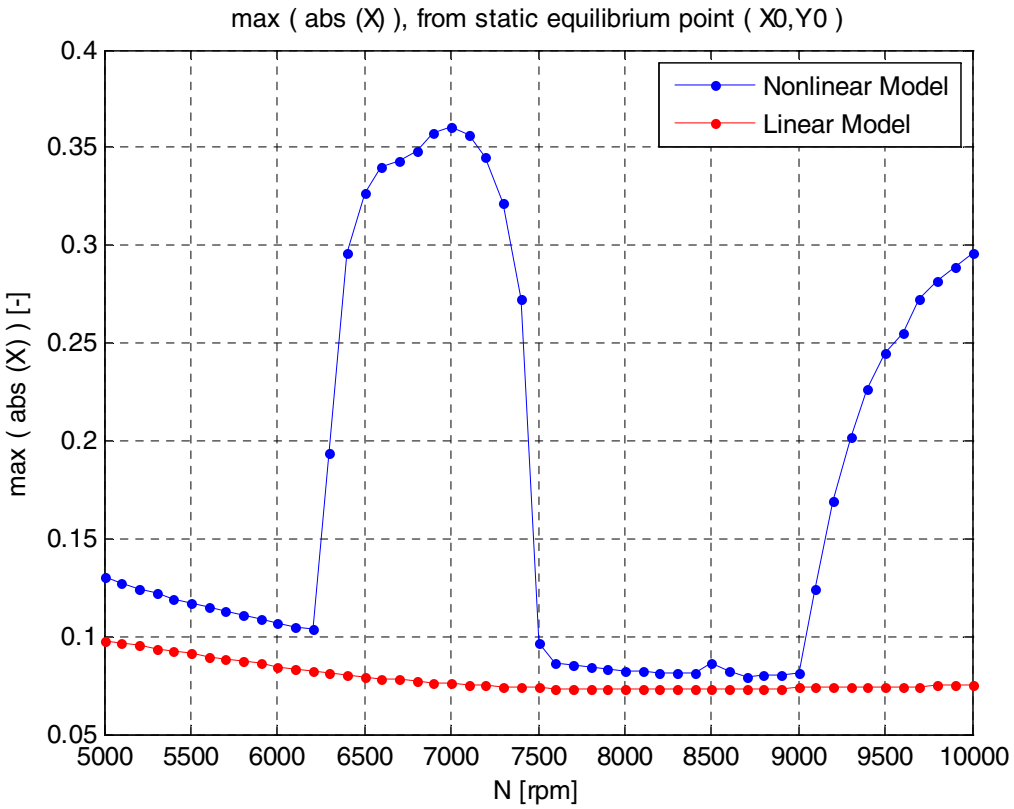

Fig 11. Maximum $\overline{X}$ displacements (linear versus nonlinear bearing model)

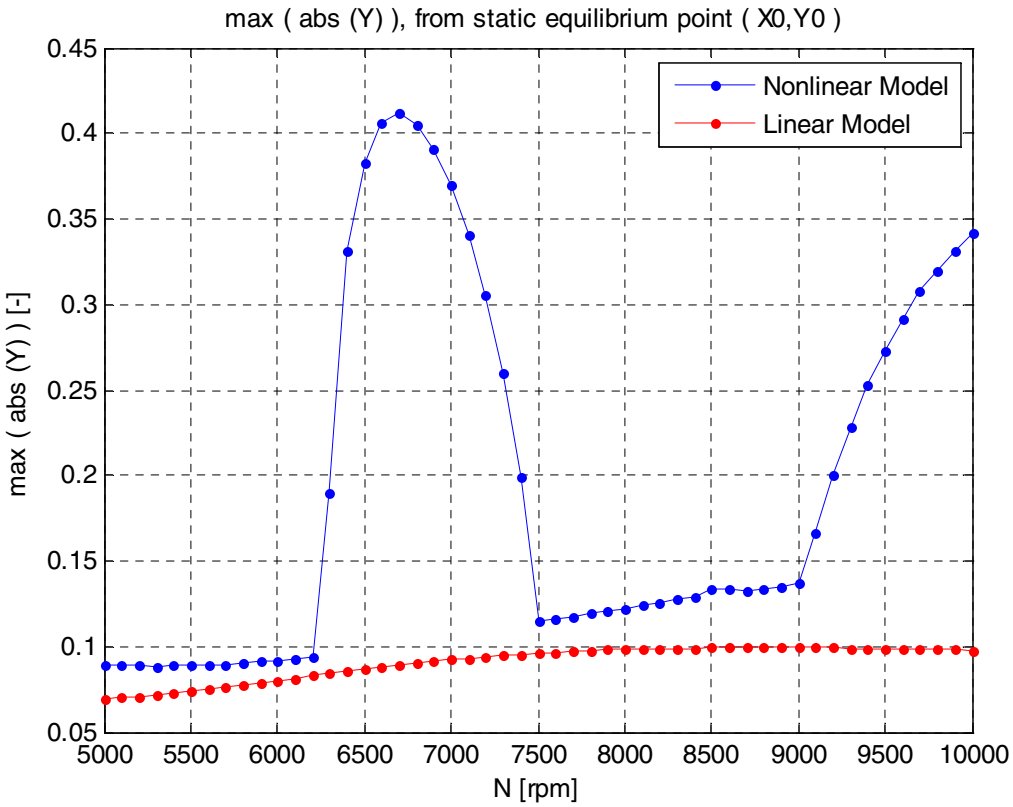

Fig 12. Maximum $\overline{Y}$ displacements (linear versus nonlinear bearing model)

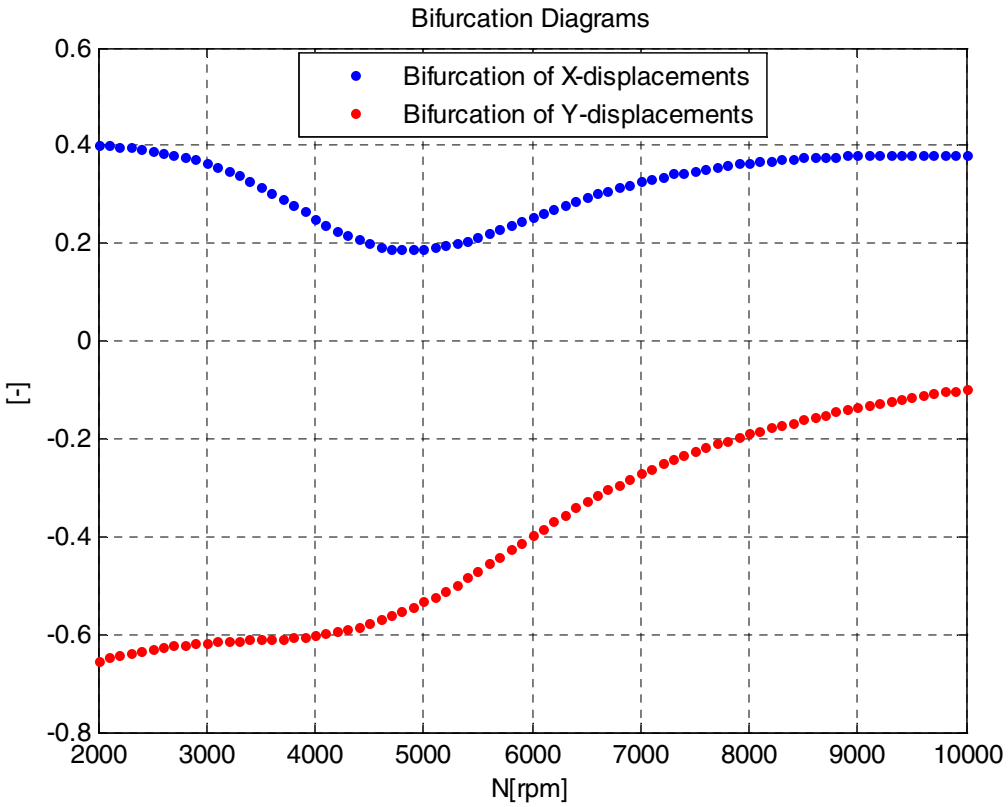

Fig 13. Bifurcation diagrams (data taken from [8]); where the bearing radial clearance $C = 50.8 \times 10^{-6}$ [m] is half that used in the case example studied

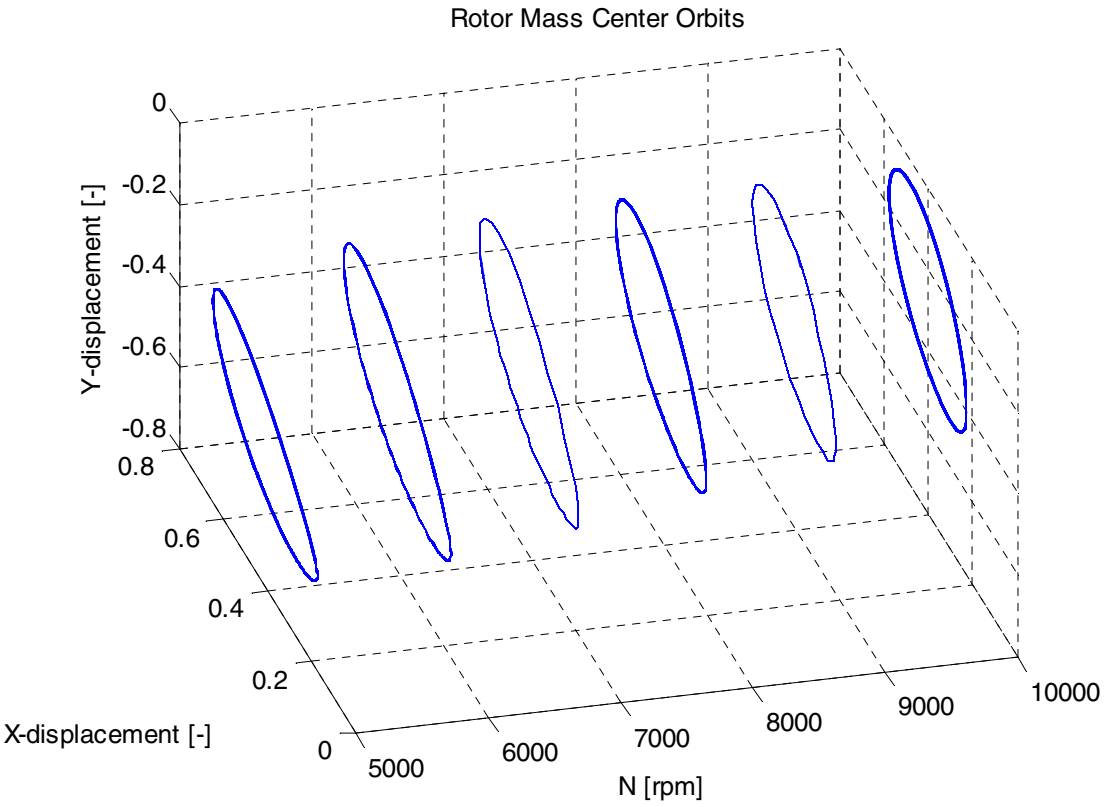

Fig 14. Rotor steady-state unbalance response (data taken from [8]); where the bearing radial clearance $C = 50.8 \times 10^{-6}$ [m] is half that used in the case example studied

.

Discussions

The results of this investigation show that linear bearing models derived from the nonlinear impedance descriptions of the Moes cavitated ($\pi - film$) finite-length bearing can predict the steady-state unbalance response of a rigid symmetric rotor supported by two identical journal-bearings at high eccentricities. However, this is only the case when operating conditions are below the threshold speed of instability (around 11400 rpm) and when the system has period one solutions. The error will also become larger closer to the resonance speed (3000 rpm), see Fig 6.
When the system has period one solutions, the trajectories predicted by linear models are in acceptable agreement with the nonlinear models. However, deviations are to be expected because the linear models will always predict elliptical trajectories, while the nonlinear models display trajectories of a banana shape and are generally asymmetrical with respect to the static equilibrium position as illustrated in [8].
As can be seen in Figures 11 and 12, the deviations in the maximum magnitudes of the $\overline{X}$ and $\overline{Y}$ displacements around the static equilibrium position are less than 30 percent in regions where the system has period one solutions (not at the resonance speed). The greatest difference in the max(abs(X,Y)) is around 0.035 and the corresponding largest max(abs(X,Y)) value is about 0.135. The smallest difference in the max(abs(X,Y)) values is around 0.015 and the corresponding largest max(abs(X,Y)) value is about 0.08. In percent, this makes the deviations into the interval (19%-26%). The deviations are expected, especially for hydrodynamic bearings operating at large eccentricities which exhibit strong nonlinear characteristics. All the other existing numerical methods for linearising the hydrodynamic bearing forces by computing the so-called bearing stiffness and damping coefficients have been proven to be inaccurate for predicting the journal trajectory at large eccentricities (see references [4,8]), and they are therefore limited at (moderate) low eccentricities (less than 0.6 according to several authors). Linear models derived from the impedance descriptions method are valid at large eccentricities. The reason for this is because they do not require any numerical differentiation or integration. They are obtained in a closed analytical form. This paper deals exclusively with journal-bearings at large eccentricity; therefore the other existing linear numerically derived models (methods) are not valid for comparisons. With differences in the range of (19%-26%), the journal trajectories from a linear model could be considered as an acceptable prediction in the present studied case where the original physical model is a strong nonlinear one.

A certain minimum speed is required to generate the hydrodynamic pressure inside the bearing clearance and therefore the rotor speed can not be zero. The case studied in this paper has a resonance at around 3000 rpm. Due to the large error expected, it is not the objective to investigate the linear model in the region around this speed (2200-4000 rpm). At low speeds, less than 2200 rpm, the journal oscillations are small due to the low unbalance force. At 1000 rpm, the journal oscillations are less than 1% of the bearing clearance and can be neglected. Therefore the low speed cases can just be considered as static due to the low unbalance excitation force. The threshold speed of instability of the journal-bearing is around 11400 rpm; therefore the system becomes unstable when running near or above this speed. The hydrodynamic lubrication will fail and metal-to-metal contact will be established if this speed is reached. The highest speed which could be reached, with unbalance force excitation in the system, is 11300 rpm. The simulations were done with rotor speeds up to 11000 rpm.

Between 6300-7500 rpm, the rotor whirls with half of its spinning frequency. Between 9000-10000 rpm, the motions are quasi periodic with regions of phase locking.

Increasing the rotor speed further, close to the threshold speed of instability (11400 rpm), the rotor system reaches instability and the hydrodynamic lubrication fails.
Figures 13 and 14 show the case with data from [8] where the system operates at low eccentricities, having only period one solutions at the displayed frequencies under the threshold speed of instability. For this case, a linear model will predict all displayed rotor trajectories (Fig14) obtained from the nonlinear bearing model.

Conclusion

Linear models derived from the nonlinear impedance descriptions of the Moes-cavitated ($\pi - film$) finite-length bearing can predict the steady-state unbalance response of a symmetric rigid rotor supported by two identical journal-bearings at high eccentricities. However, this is only the case where operating conditions are below the threshold speed of instability and when the system has period one solutions. The error will also increase closer to the resonance speed.
The deviations in the maximum magnitudes of the $\overline{X}$ and $\overline{Y}$ displacements about the static equilibrium position are in the interval between approximately 19% and 26% when the system has period one solutions, except at the resonance speed. These deviations depend on the net difference in shapes between the two respective rotor trajectories and also on the fact that the nonlinear models generate trajectories which are generally asymmetrical with respect to the static equilibrium position.
This paper concerns the dynamics of a bearing model with L/D = 0.25 at high eccentricities. However, the described procedure is general and may be used in investigations of systems with bearings of other L/D ratios

References

[1] Ram Turaga, A. S. Sekhar, and B. C. Majumdara, 1999, “Comparison between Linear and Nonlinear Transient analysis Techniques to Find the Stability of a Rigid Rotor’’,
Journal of Tribology, Transactions of the ASME, Vol. 121, pp. 198-201 (1999)
[2] A. K. Tieu and Z. L. Qiu, 1994, “Stability of Finite Journal Bearings from Linear and Nonlinear Bearing Forces’’, Tribology Transactions, Vol. 38(1995), 3, pp. 627-635
[3] J. W. Lund and Thomsen, 1978, “A Calculation Method and Data for the Dynamic Coefficients of Oil-Lubricated Journal Bearings’’, Topics in Fluid Bearing and Rotor Bearing System, ASME, New York, (1978), pp. 1-28
[4] D. Childs, “Turbomachinery Rotordynamics: Phenomena, Modeling, & Analysis’’,
Wiley-Interscience, 1993, ISBN 0-471-53840-X, Chapter 3
[5] R. D. Brown, G. Drummond and P. S. Addison 1999 “Chaotic response of a short journal bearing’’, IMechE 2000, Vol. 214, Part J
[6] D. Childs, H. Moes, H. van Leeuwen, 1977, “Journal bearing impedance descriptions for rotordynamic applications’’, Journal of Lubrication Technology, Transactions of the ASME, April 1977, pp. 198-214
[7] Moes and R. Bosma, 1981, “Mobility and impedance definitions for plain journal bearings’’,
Journal of Lubrication Technology, Transactions of the ASME, Vol. 103, pp. 468-470 (1981)
[8] Wen Jeng Chen, Edgar J. Gunter, “Introduction to Dynamics of Rotor-Bearing Systems’’,
Trafford Publishing, 2007, ISBN 978-1-4120-5190-3, Chapter 6

Appendix A

$$
\begin{cases}
W_0 = \left[0.15\left(E_0{}^2 + G_0{}^2\right)^{\frac{1}{2}}\left(1-\xi_0\right)^{\frac{3}{2}} \right]^{-1} \\
E_0 = 1 + 2.12Q_0 \\
G_0 = 3\eta_0 \dfrac{\left(1+3.6Q_0\right)}{4\left(1-\xi_0\right)} \\
Q_0 = \left(1-\xi_0\right)\left(\dfrac{L}{D}\right)^{-2} \\
\xi_0 = \varepsilon_0 \cos\gamma_0 \\
\eta_0 = \varepsilon_0 \sin\gamma_0 \\
\gamma_0 \cong \left\{1-\xi'\left(1-\eta'^2\right)^{\frac{1}{2}}\right\}\left[\tan^{-1}\left\{ \dfrac{4\left(1+2.12B_0\right)\left(1-\eta'^2\right)^{\frac{1}{2}}}{3\left(1+3.6B_0\right)\eta'} \right\} - \dfrac{\pi}{2}\dfrac{\eta'}{|\eta'|} + \sin^{-1}\eta' \right] + \alpha_0 - \sin^{-1}\eta' \\
B_0 = \left(1-\varepsilon_0{}^2\right)\left(\dfrac{L}{D}\right)^{-2} \\
\xi' = \varepsilon_0 \cos\alpha_0 \\
\eta' = \varepsilon_0 \sin\alpha_0 \\
\alpha_0 = \dfrac{\pi}{2}
\end{cases}
$$

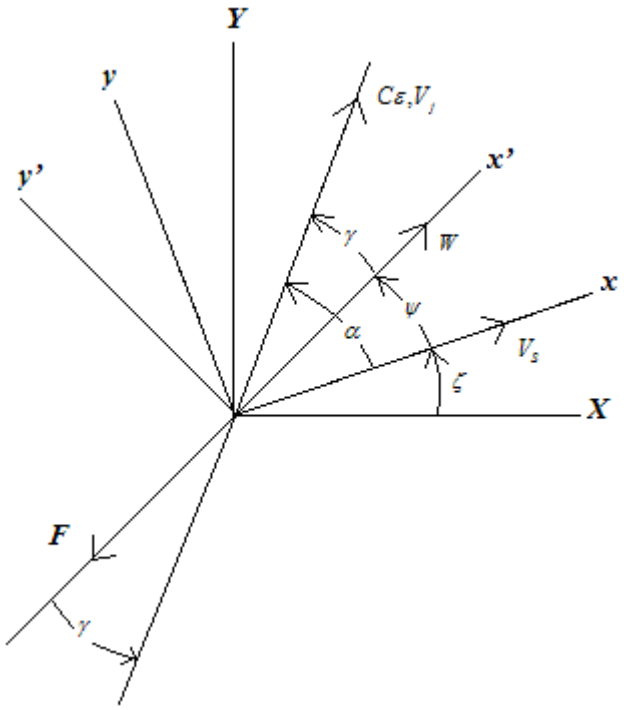

Fig 15. Kinematic variables for impedances and mobilities (from [6] and [4])

Appendix B

$$\left(\frac{\partial\gamma}{\partial\varepsilon}\right)_{\alpha}=\frac{4}{3}\left[2(b-a)b^{-2}-a\frac{{\varepsilon_0}^{-2}}{b}\right]\cos^2\gamma_0\left(1-{\varepsilon_0}^2\right)^{-\frac{1}{2}}$$

$$\begin{cases}a=1+2.12B_0\\ b=1+3.6B_0\end{cases}$$

$$\left(\frac{\partial W}{\partial\varepsilon}\right)_{\alpha}=\left(\frac{\partial W}{\partial\xi}\right)_{\eta}\left(\frac{\partial\xi}{\partial\varepsilon}\right)_{\alpha}+\left(\frac{\partial W}{\partial\eta}\right)_{\xi}\left(\frac{\partial\eta}{\partial\varepsilon}\right)_{\alpha}$$

$$\begin{cases}\left(\dfrac{\partial W}{\partial\xi}\right)_{\eta}=-W_0\left[\left(E_0^2+G_0^2\right)^{-1}\left\{\dfrac{3}{4}G_0\eta_0d^{-2}-2.12E_0\left(\dfrac{L}{D}\right)^{-2}\right\}-\dfrac{3}{2}d\right]\\ d=1-\xi_0\\ \left(\dfrac{\partial W}{\partial\eta}\right)_{\xi}=-W_0\left(E_0^2+G_0^2\right)^{-1}\dfrac{G_0^2}{\eta_0}\\ \left(\dfrac{\partial\xi}{\partial\varepsilon}\right)_{\alpha}=\cos\gamma_0-\varepsilon_0\sin\gamma_0\left(\dfrac{\partial\gamma}{\partial\varepsilon}\right)_{\alpha}\\ \left(\dfrac{\partial\eta}{\partial\varepsilon}\right)_{\alpha}=\sin\gamma_0+\varepsilon_0\cos\gamma_0\left(\dfrac{\partial\gamma}{\partial\varepsilon}\right)_{\alpha}\end{cases}$$

$$\left(\frac{\partial\gamma}{\partial\alpha}\right)_{\varepsilon}=1+\left[\gamma_0-\frac{\pi}{2}+\sin^{-1}\varepsilon_0\right]\varepsilon_0\left(1-{\varepsilon_0}^2\right)^{-\frac{1}{2}}$$

$$\left(\frac{\partial W}{\partial\alpha}\right)_{\varepsilon}=\left(\frac{\partial W}{\partial\gamma}\right)_{\varepsilon}\left(\frac{\partial\gamma}{\partial\alpha}\right)_{\varepsilon}$$

$$\begin{cases}\left(\dfrac{\partial W}{\partial\gamma}\right)_{\varepsilon}=\left(\dfrac{\partial W}{\partial\xi}\right)_{\eta}\left(\dfrac{\partial\xi}{\partial\gamma}\right)_{\varepsilon}+\left(\dfrac{\partial W}{\partial\eta}\right)_{\xi}\left(\dfrac{\partial\eta}{\partial\gamma}\right)_{\varepsilon}\\ \left(\dfrac{\partial\xi}{\partial\gamma}\right)_{\varepsilon}=-\varepsilon_0\sin\gamma_0\\ \left(\dfrac{\partial\eta}{\partial\gamma}\right)_{\varepsilon}=\varepsilon_0\cos\gamma_0\end{cases}$$